JACS
JOURNAL OF THE AMERICAN CHEMICAL SOCIETY
pubs.acs.org/JACS
Article

Transient Triplet Metallopnictinidenes M−Pn (M = Pd^{II}, Pt^{II}; Pn = P, As, Sb): Characterization and Dimerization

Marc C. Neben,[&] Nils Wegerich,[&] Tarek A. Al Said, Richard R. Thompson, Serhiy Demeshko, Kevin Dollberg, Igor Tkach, Gerard P. Van Trieste, III, Hendrik Verplancke, Carsten von Hänisch,* Max C. Holthausen,* David C. Powers,* Alexander Schnegg,* and Sven Schneider*

Cite This: J. Am. Chem. Soc. 2025, 147, 5330−5339

Read Online

ACCESS | Metrics & More | Article Recommendations | Supporting Information

ABSTRACT: Nitrenes (R−N) have been subject to a large body of experimental and theoretical studies. The fundamental reactivity of this important class of transient intermediates has been attributed to their electronic structures, particularly the accessibility of triplet vs singlet states. In contrast, electronic structure trends along the heavier pnictinidene analogues (R−Pn; Pn = P−Bi) are much less systematically explored. We here report the synthesis of a series of metallodipnictenes, {M−Pn═Pn−M} (M = Pd^{II}, Pt^{II}; Pn = P, As, Sb, Bi) and the characterization of the transient metallopnictinidene intermediates, {M−Pn} for Pn = P, As, Sb. Structural, spectroscopic, and computational analysis revealed spin triplet ground states for the metallopnictinidenes with characteristic electronic structure trends along the series. In comparison to the nitrene, the heavier pnictinidenes exhibit lower-lying ground state SOMOs and singlet excited states, thus suggesting increased electrophilic reactivity. Furthermore, the splitting of the triplet magnetic microstates is beyond the phosphinidenes {M−P} dominated by heavy pnictogen atom induced spin−orbit coupling.

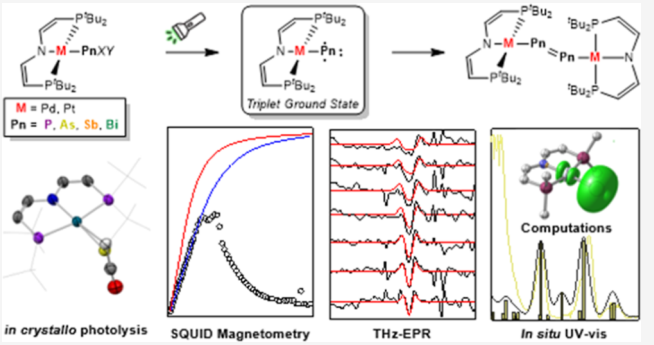

INTRODUCTION

Nitrenes (N−R), are key reactive intermediates in chemical synthesis and, as such, usually transient species.[1] Nevertheless, a substantial body of matrix isolation, transient spectroscopy, and computational studies could connect the fundamental reactivity of these subvalent species to their spin state energetics.[2] Parent imidogen (N−H) is a prototypical axial diradical with two electrons in two localized, degenerate, and orthogonal orbitals.[3] In consequence, the lowest electronic configuration $1\sigma^2 2\sigma^2 3\sigma^2 1\pi^2$ gives rise to a triplet ground ($^3\Sigma^-$) and two singlet excited states ($^1\Delta$ and $^1\Sigma^+$).[4] Simple alkyl- and arylnitrenes exhibit the same state ordering with a ground state that is moderately split by dipolar spin interactions ($D \approx 1-2$ cm^{-1}).[5,6] Excessive steric shielding recently enabled the isolation of persistent triplet arylnitrenes (Figure 1a).[7] In turn, the singlet electromer is stabilized by breaking the π_N orbital degeneracy,[8] and Bertrand could isolate a singlet nitrene with a strong, unidirectional π-push substituent (Figure 1a).[9]

In contrast to nitrenes, the heavier pnictinidenes, Pn−R (Figure 1b; Pn = P, As, Sb, Bi), are much less well explored.[10] Computational studies predicted a triplet ground state for methylphosphinidene, P−Me, but facile isomerization via the lower lying singlet states[11] prevented its spectroscopic confirmation until very recently.[12] EPR characterization of a triplet phoshinidene (P−Mes) was first reported in 1994;[13] matrix isolation studies of transient arylphosphinidenes and -arsinidenes even much more recently.[14] Sb−Ph and Bi−Ph remain elusive. Triplet Bi−Me could recently be detected in the gas-phase.[15] The installation of bulky aryl substituents also enabled the isolation of the heaviest triplet pnictinidenes (Figure 1b),[16,17] while the analogous phosphinidene proved unstable toward intramolecular decay.[18] However, in analogy to nitrenes a strong π-donor substituent gave rise to an isolable singlet phosphinidene (Figure 1b).[19]

Notably, the heavier triplet pnictinidenes showcase an increasing impact of relativistic effects. For example, Cornella's bismuthinidene (Figure 1b) exhibits a nonmagnetic triplet ground state owing to huge spin−orbit coupling (SOC) induced zero-field-splitting (ZFS) of more than +5400 cm^{-1}.[16,20] Thus, SOC-induced stabilization is of a magnitude that not only dominates the spectroscopic and magnetic properties, but might be of direct relevance for chemical

Received: November 26, 2024
Revised: January 7, 2025
Accepted: January 13, 2025
Published: January 29, 2025

https://doi.org/10.1021/jacs.4c16830
J. Am. Chem. Soc. 2025, 147, 5330−5339

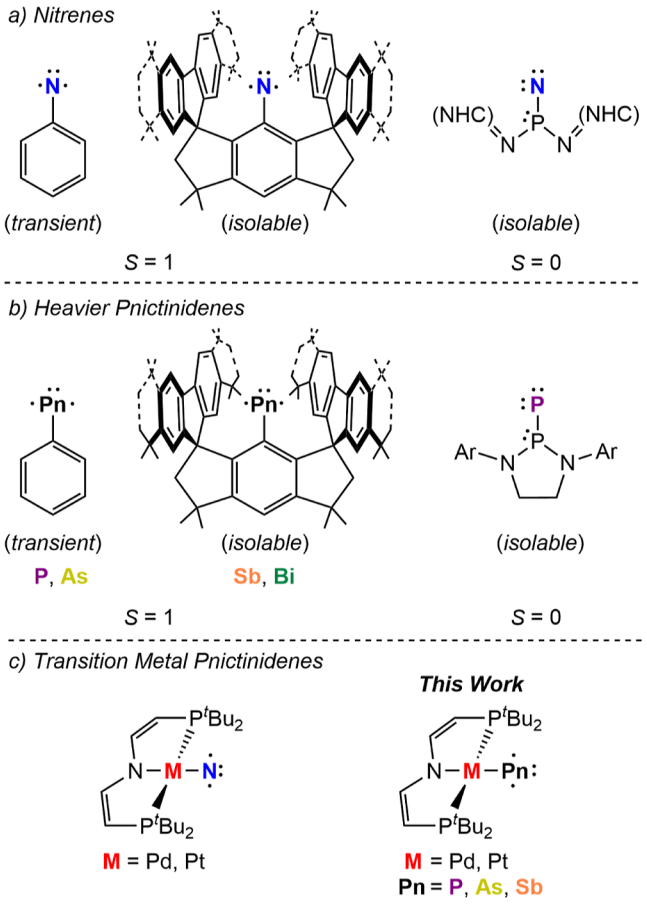

Figure 1. Selected examples of nitrenes, R−N (a) and heavier pnictinidenes, R−Pn (b) versus the metallopnictinidenes presented here (c).

reactivity. Systematic studies of these electronic structure trends are of key importance to support the current emergence of redox catalysis mediated by heavy main group elements.[21]

While azide dissociation is most common for nitrene generation, alternative strategies are required for the heavier analogues. Thermal or photochemical fragmentation of precursors, like $^{t}Bu_2P{-}P{=}PBr^{t}Bu_2$, phospholenes, phosphiranes, or dibenzophosphanorbornadienes, are versatile routes to transient phosphinidenes.[10,22] The heavier pnictinidenes are commonly synthesized upon reduction of Pn^{III} (pseudo)-halides.[16,17] Furthermore, pnictaethynolate anions ($PnCO^-$, Pn = P, As)[23] have recently emerged as versatile reagents for pnictogen atom transfer to transition metals.[24] CO dissociation gave rise to pnictide complexes with M≡P triple bonds and dipnictene (M−Pn=Pn−M) coupling products.[25] However, heavier authentic metallopnictinidenes (M−Pn), which are analogous to organic triplet pnictinidenes with a limiting electronic configuration that represents M−Pn single bonding, remain elusive.[26]

Our groups recently reported the synthesis of the formal group 10 nitrido complexes, [M(N)(PNP)] [M = Pd, Pt; PNP = $N(CHCHP^{t}Bu_2)_2$; Figure 1c],[27] as authentic metallonitrenes (M−N) with a univalent nitrogen diradical ligand that is singly bound to closed shell M^{II} ions. Furthermore, photolysis of the phosphaethynolate complex [Pt(PCO)(PNP)] ($\mathbf{1}^{Pt,P}$, Scheme 1) gave the pnictide coupling product [(P_2){Pt(PNP)}$_2$] ($\mathbf{2}^{Pt,P}$),[28] suggesting a transient metallophosphinidene intermediate. We here report the synthesis of the full heavier metallodipictene series, [(Pn_2){M(PNP)}$_2$] (Pn = P−Bi) as well as the *in situ* characterization of the pnictinidene intermediates, [M(Pn)(PNP)}] (Pn = P−Sb), providing systematic electronic structure trends along the series.

Scheme 1. Photoinduced Pnictide Coupling; Reaction Conditions: (a) $\mathbf{2}^{Pd,P}$: λ = 456 nm, Benzene, 3 h, Room Temperature, 87% Yield; (b) $\mathbf{2}^{Pt,P}$: see ref 28; (c) $\mathbf{2}^{Pd,As}$: λ = 525 nm, THF, 90 min, 0 °C, 82% Yield; (d) $\mathbf{2}^{Pt,As}$: λ = 525 nm, Toluene, 30 min, −30 °C; 87% Yield; (e) $\mathbf{2}^{Pt,Sb}$: λ = 370 nm, 2-Methyl THF, 6 h, −196 °C; 84% Yield; (f) $\mathbf{2}^{Pt,Bi}$: λ = 370 nm, Toluene, 16 h,−40 °C, 25% Yield

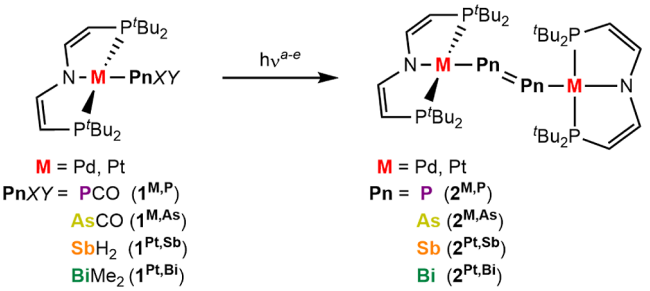

RESULTS AND DISCUSSION

Precursor Syntheses. In analogy to previously reported $\mathbf{1}^{Pt,P}$,[28] the diamagnetic precursors [M(PnCO)(PNP)] ($\mathbf{1}^{M,Pn}$; M = Pd, Pt; Pn = P, As; Scheme 1) were obtained in near quantitative yields by salt metathesis from the divalent group 10 triflates with [Na(diox)$_n$]PnCO (Pn = P, As). Structural characterization of all products by single-crystal X-ray diffraction (see Supporting Information) showed marginal variations within the M(PNP) fragments. The smaller M−Pn−C angles for Pn = As [$\mathbf{1}^{Pd,As}$: 95.87(15)°, $\mathbf{1}^{Pt,As}$: 99.0(3)°] versus P [$\mathbf{1}^{Pd,P}$: 99.63(3)°, $\mathbf{1}^{Pt,P}$: 101.74(11)°] are in line with increased pnictogen p-character in M−PnCO bonding.[29] All complexes feature absorption bands in the visible range at around 500−600 nm, which can be assigned to electronic LMCT(PnCO → M) transitions (cf. Supporting Information for further details).

The lack of the heaviest pnictaethynolate precursors required alternative strategies for Sb and Bi.[30] The Liddle group prepared thorium stibinidene and stibido complexes, starting from SbH_2^-.[31] Motivated by this work, we synthesized the parent stibanide complex [Pt(SbH_2)(PNP)] ($\mathbf{1}^{Pt,Sb}$, Scheme 1) with [K(18-crown-6)(thf)SbH_2].[32] Isolation of the Pd analogue was not successful due to low thermal stability. The SbH_2 substituent of $\mathbf{1}^{Pt,Sb}$ exhibits a ^{1}H NMR signal at $\delta = -0.94$ ppm, comparing well with reported primary stibanes.[33] The Sb−H stretching modes are assigned to a broad IR band at $\tilde{\nu} = 1834$ cm^{-1}, which is blue-shifted versus the potassium salt ($\Delta\tilde{\nu} = 60$ cm^{-1}). $\mathbf{1}^{Pt,Sb}$ exhibits an absorption band in the near-UV region ($\lambda_{max} = 318$ nm) that is assigned to a $\pi_{C=C} \rightarrow \pi^*_{C=C}$ transition in the pincer ligand backbone upon comparison with [Pt(N_3)(PNP)].[34]

As BiH_2^- is highly unstable, we resorted to organobismuth analogues, which can be generated from triorganobismuthanes with alkali metal.[35] Thermal Bi−C homolysis of $BiMe_3$ has been reported at moderate temperatures (60−120 °C).[15] Salt metathesis of [Pt(OTf)(PNP)] with *in situ* generated $BiMe_2^-$ gave a product in up to 90% ^{31}P NMR spectroscopic yield that is assigned to [Pt($BiMe_2$)(PNP)] ($\mathbf{1}^{Pt,Bi}$) based on mass spectrometry and single crystal X-ray diffraction (Figure 2).

https://doi.org/10.1021/jacs.4c16830
J. Am. Chem. Soc. 2025, 147, 5330−5339

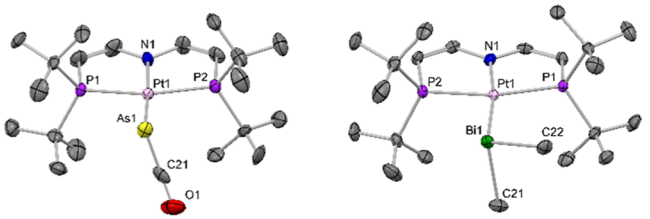

Figure 2. Molecular structure of $\mathbf{1}^{\mathbf{Pt,As}}$ (left) and $\mathbf{1}^{\mathbf{Pt,Bi}}$ (right) with thermal ellipsoids at the 50% probability level. H atoms are omitted for clarity. Selected bond lengths [Å] and angles [°]:$\mathbf{1}^{\mathbf{Pt,As}}$ Pt1−As1:2.455(1); Pt1−As1−C21:99.0(3); $\mathbf{1}^{\mathbf{Pt,Bi}}$: Pt1−Bi1:2.7323(3); Pt1−Bi1−C21:99.69(15), Pt1−Bi1−C22:117.53(14), C21−Bi1−C22:91.7(2).

The molecular structure of $\mathbf{1}^{\mathbf{Pt,Bi}}$ reveals a long Pt−Bi bond [2.7323(3) Å] and almost orthogonal methyl groups [C−Bi−C: 91.7(2)°], which is in line with purely p_{Bi} orbital contributions to bonding [cf. Supporting Information for a detailed natural bond orbital (NBO) analysis]. Notably, $\mathbf{1}^{\mathbf{Pt,Bi}}$ is the first structurally characterized transition metal diorganobismuthyl complex.[36] Besides $\mathbf{1}^{\mathbf{Pt,Bi}}$, a side product (10−15%) is observed. The small $^{1}J_{Pt-P}$ coupling constant (469 Hz) suggests high-valent Pt, e.g., due to oxidative addition to Pt^{II}.[37] While identification and separation of the side product unfortunately remained unsuccessful, the mixture could be directly used as precursor for dibismuthene synthesis (see below).

Photolytic Pnictide Coupling. In the absence of light, the phosphorus precursors $\mathbf{1}^{\mathbf{Pd,P}}/\mathbf{1}^{\mathbf{Pt,P}}$ are stable in solution at room temperature over several days. The other precursors slowly decay at these conditions giving either the respective pnictide coupling products (see below) as main products or lead to undefined decomposition in case of $\mathbf{1}^{\mathbf{Pt,Sb}}$. Photolysis was carried out in solution, guided by the thermal and spectroscopic properties of the respective precursors (Scheme 1). For $\mathbf{1}^{\mathbf{Pd,P}}/\mathbf{1}^{\mathbf{Pd,As}}$ and $\mathbf{1}^{\mathbf{Pt,P}}/\mathbf{1}^{\mathbf{Pt,As}}$, decay of the characteristic ν(PnCO) IR band confirmed the conversion of the precursors over 1−3 h with concomitant growth of new electronic absorption features in the visible range. As previously reported for $\mathbf{1}^{\mathbf{Pt,P}}$,[28] the Pd^{II} and Pt^{II} metallodipnictene products [(μ-Pn_2){M(PNP)}$_2$] ($\mathbf{2}^{\mathbf{M,Pn}}$; M = Pd, Pt; Pn = P−Sb) could be isolated in yields beyond 80%, while significantly smaller yields (~25%) were obtained for $\mathbf{2}^{\mathbf{Pt,Bi}}$. All coupling products proved thermally stable at room temperature in solution and in the solid state. Note that the analogous diazenido complex [(μ-N_2){Pt(PNP)}$_2$] readily loses N_2 at low temperatures.[38] Heavier dipnictenes, R−Pn=Pn−R, with organic, main group, and transition metal substituents are well-known for Pn = P−Sb.[25a,28,33,39] In contrast, only few dibismuthenes (R−Bi=Bi−R) have been reported,[16a,39,40] as well some metal compounds of the Bi_2^{2-} and Bi_2^{3-} radical anions.[41,42]

The broad ^{31}P NMR signal at δ_P = +784 ppm is assigned to the P_2-bridged Pd complex $\mathbf{2}^{\mathbf{Pd,P}}$, supporting P=P double bond character, as for previously reported $\mathbf{2}^{\mathbf{Pt,P}}$ (δ_P = +707 ppm).[28] NMR spectroscopic characterization of $\mathbf{2}^{\mathbf{Pt,Bi}}$ was unfortunately impeded by the extremely low solubility in common organic solvents. All coupling products were characterized by single-crystal X-ray diffraction (Figure 3). Comparison with Pyykkö's covalent bond radii[43] and computed Wiberg bond indices support Pn=Pn double bonding. The elongation of the Pn=Pn bonds from $\{P_2\}^{2-}$ to $\{Bi_2\}^{2-}$ is in line with the increasing valence orbital

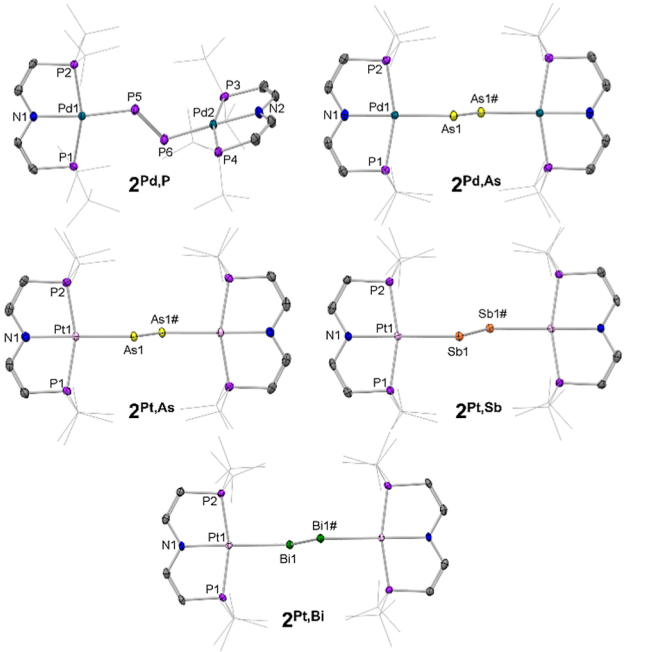

	Pn–Pn [Å]	M–Pn–Pn [°]		Pn–Pn [Å]	M–Pn–Pn [°]
$\mathbf{2}^{\mathbf{Pt,P}}$	2.037(2)	108.30(8) 119.22(9)	$\mathbf{2}^{\mathbf{Pd,As}}$	2.2698(7)	115.08(2)
$[\mathbf{2}^{\mathbf{Pt,P}}]^{+}$	1.984(5)	121.7(2) 133.8(2)	$\mathbf{2}^{\mathbf{Pt,As}}$	2.2888(9)	115.55(3)
$[\mathbf{2}^{\mathbf{Pt,P}}]^{2+}$	1.864(2)	162.67(6)	$\mathbf{2}^{\mathbf{Pt,Sb}}$	2.6638(7)	111.32(2)
$\mathbf{2}^{\mathbf{Pd,P}}$	2.015(2)	107.00(6) 119.95(7)	$\mathbf{2}^{\mathbf{Pt,Bi}}$	2.8400(4)	108.73(2)

Figure 3. Molecular structures and selected structural parameters of the dipnictenes with thermal ellipsoids at the 50% probability level. H atoms and disordered atoms are omitted and ^{t}Bu-groups represented as sticks for clarity. Structural parameters of $\mathbf{2}^{\mathbf{Pt,P}}$, $[\mathbf{2}^{\mathbf{Pt,P}}]^{+}$, and $[\mathbf{2}^{\mathbf{Pt,P}}]^{2+}$ taken from ref 28.

expansion (see Supporting Information for detailed results of NBO analysis).[29,44] Accordingly, the As=As stretching vibrations [$\tilde{\nu}_{exp}$ = 308 ($\mathbf{2}^{\mathbf{Pd,As}}$) and 302 cm^{-1} ($\mathbf{2}^{\mathbf{Pt,As}}$)] are red-shifted vs P=P [$\tilde{\nu}_{exp}$ = 585 ($\mathbf{2}^{\mathbf{Pd,P}}$) and 582 cm^{-1} ($\mathbf{2}^{\mathbf{Pt,P}}$)]. While the Sb=Sb and Bi=Bi stretching modes could not be reliably assigned from experiment, DFT computations confirmed the trend for the full series [$\tilde{\nu}_{DFT}/cm^{-1}$ = 561 ($\mathbf{2}^{\mathbf{Pt,P}}$), 314 ($\mathbf{2}^{\mathbf{Pt,As}}$), 204 ($\mathbf{2}^{\mathbf{Pt,Sb}}$), 149 ($\mathbf{2}^{\mathbf{Pt,Bi}}$)]. This picture is complemented by comparison of the dipole allowed electronic $\pi(Pn_2) \rightarrow \pi^*(Pn_2)$ transitions ($\mathbf{2}^{\mathbf{Pt,P}}$: 22,400, $\mathbf{2}^{\mathbf{Pt,As}}$: 21,400, $\mathbf{2}^{\mathbf{Pt,Sb}}$: 20,100, $\mathbf{2}^{\mathbf{Pt,Bi}}$: 16,800 cm^{-1}; see Supporting Information for Pd complexes), which were assigned upon comparison with TD-DFT calculations.

The cyclic voltammogram of $\mathbf{2}^{\mathbf{Pt,As}}$ (Figure 4b) features a reversible oxidation, which is anodically shifted by ΔE^0 = 0.15 V with respect to P-analogue $\mathbf{2}^{\mathbf{Pt,P}}$,[28] supporting a higher lying highest occupied molecular orbital (HOMO) of the diarsene complex. In contrast to $\mathbf{2}^{\mathbf{Pt,P}}$, further oxidations are fully irreversible at scan rates up to 4 $V \cdot s^{-1}$, preventing synthetic access to a stable dication with a neutral As≡As bridge. However, chemical oxidation of $\mathbf{2}^{\mathbf{Pt,As}}$ with decamethylferrocenium enabled the isolation of the monocationic radical complex [(μ-As_2){Pt(PNP)}$_2$]$^{+}$ ($[\mathbf{2}^{\mathbf{Pt,As}}]^{+}$) in 91% yield (Figure 4a). The Q-band EPR spectrum of $[\mathbf{2}^{\mathbf{Pt,As}}]^{+}$ in frozen methyltetrahydrofuran (Figure 4c) shows a rhombic signal with large g-anistropy (2.183, 1.959, 1.764), which reflects that

https://doi.org/10.1021/jacs.4c16830
J. Am. Chem. Soc. 2025, 147, 5330−5339

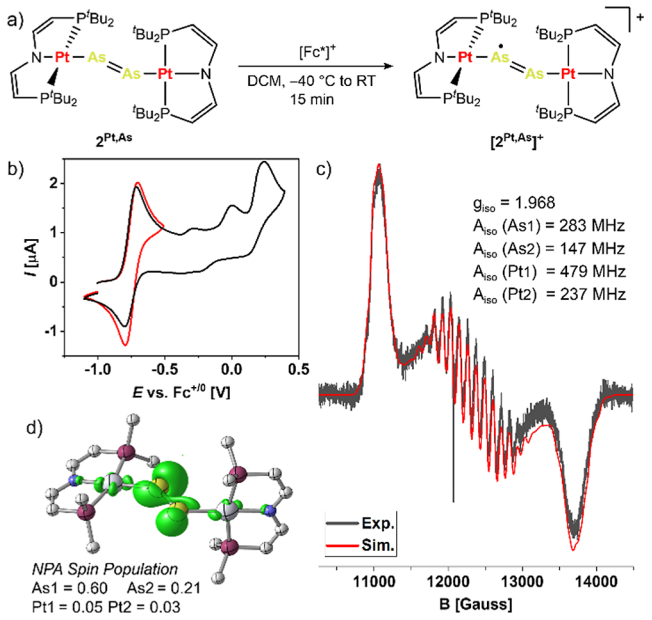

Figure 4. (a) Synthesis of radical complex $[\mathbf{2}^{\mathbf{Pt,As}}]^+$. (b) Cyclic voltammogram of $\mathbf{2}^{\mathbf{Pt,As}}$ in PhF. (c) Continuous wave *Q*-band EPR spectrum (black) and simulation (red with simulation parameters) of $[\mathbf{2}^{\mathbf{Pt,As}}]^+$ in MeTHF at 40 K. (d) NPA spin population of $[\mathbf{2}^{\mathbf{Pt,As}}]^+$.

of $[(\mu\text{-}P_2)\{Pt(PNP)\}_2]^+$ with a bridging $\{P_2\}^-$ radical ligand.[28] The notion of an As_2-centered π-radical is further supported by large, anisotropic ^{75}As hyperfine interaction, as well as quantum-chemical spin population analyses, which assign less than 10% of the spin density to the Pt atoms. Accordingly, removal of an electron from $\mathbf{2}^{\mathbf{Pt,As}}$ [HOMO: π^* (As_2)] results in a hypsochromic shift of the As═As stretching vibration ($\Delta\tilde{\nu}_{exp}$ = +38 cm^{-1}) similar to the reported diphosphenyl radical ($\Delta\tilde{\nu}_{exp}$ = +44 cm^{-1}).[28] Electrochemical characterization of the heavier metallodipnictenes $\mathbf{2}^{\mathbf{Pt,Sb}}$ and $\mathbf{2}^{\mathbf{Pt,Bi}}$ was prevented by their poor solubility. Nevertheless, the spectroscopic data of $[\mathbf{2}^{\mathbf{Pt,As}}]^+$ fully supports the electronic structure model obtained for the pnictide coupling products.

Structural Characterization of the Metallopnictinidenes. Having established light-induced pnictide coupling, the putative metallopnictinidene intermediates were examined. The spectroscopic observation of CO (P, As) and H_2 (Sb) upon irradiation of the precursor complexes supports the primary formation of metallopnictinidenes. In contrast, no ethane was detected upon photolysis of $\mathbf{1}^{\mathbf{Pt,Bi}}$. Thus, direct reductive elimination can be ruled out. $BiMe_3$ exhibits a propensity for radical reactions upon Me_2Bi–Me homolysis due to a small Bi–C bond dissociation energy around 50 kcal·mol^{-1}.[15] However, the mechanism that leads to dibismuthene $\mathbf{2}^{\mathbf{Pt,Bi}}$ ultimately remains unknown. The bismuth precursor was therefore not included in further examinations of transient metallopnictinidenes.

We first pursued *in crystallo* photolysis studies, which has proven effective for the structural characterization of related transient species.[27,45] Site isolation within the crystal lattice prevents bimolecular decay as observed during solution-phase photolysis. Mounted single crystals of $\mathbf{1}^{\mathbf{Pd,P}}$, $\mathbf{1}^{\mathbf{Pd,As}}$, $\mathbf{1}^{\mathbf{Pt,P}}$, and $\mathbf{1}^{\mathbf{Pt,As}}$, respectively, were photolyzed at 100 K with an light-emitting diode (λ = 365 nm) and the diffraction data acquired with synchrotron radiation (λ = 0.41328 Å). Refinement of the data for $\mathbf{1}^{\mathbf{Pd,P}}$ and $\mathbf{1}^{\mathbf{Pt,P}}$ indicated about 40% photoconversion to the phosphinidenes [M(P)(PNP)] [M = Pd ($\mathbf{3}^{\mathbf{Pd,P}}$), Pt ($\mathbf{3}^{\mathbf{Pt,P}}$)], while the arsinidenes [M(As)(PNP)] [M = Pd ($\mathbf{3}^{\mathbf{Pd,As}}$), Pt ($\mathbf{3}^{\mathbf{Pt,As}}$)] were obtained in lower yields around 15% (Figure 5). Further irradiation led to sample degradation and

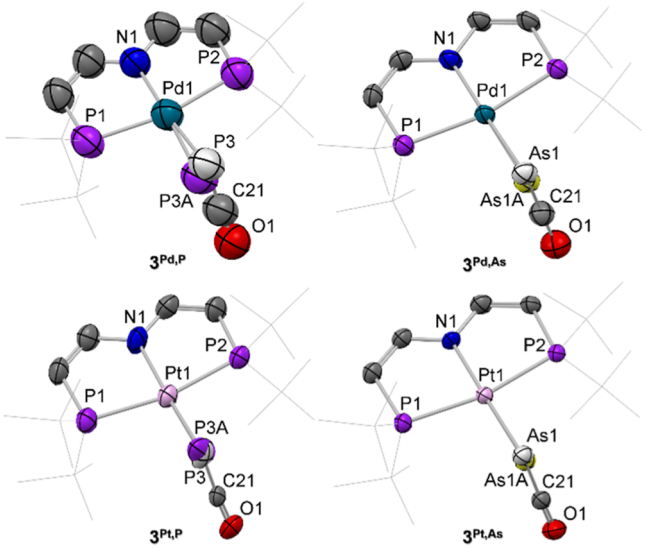

Figure 5. Overlays of the molecular structures of the precursor complexes and the respective metallopnictinidenes from crystal-to-crystal transformation experiments; thermal ellipsoids at the 50% probability level. H atoms are omitted and ^{t}Bu-groups drawn as sticks for clarity. Selected bond lengths [Å]: $\mathbf{3}^{\mathbf{Pd,As}}$ Pd1–As1A, 2.349(13); $\mathbf{3}^{\mathbf{Pt,P}}$ Pt1–P3A, 2.25(4); $\mathbf{3}^{\mathbf{Pt,As}}$ Pt1–As1A 2.36(3).

loss of crystallinity. Due to significantly larger experimental errors, the bond metrics of $\mathbf{3}^{\mathbf{Pd,P}}$ will not be discussed. All attempts to obtain suitable single crystals of the antimonide complex $\mathbf{1}^{\mathbf{Pt,Sb}}$ were unfortunately unsuccessful, excluding the stibinidene from crystallographic characterization. However, only minor structural perturbation can be expected to result from H_2 elimination, anyway.

Light-induced CO elimination is accompanied by significant contraction of the Pt–P bond length (Δd = −0.11 Å) from 2.3574(16) Å ($\mathbf{1}^{\mathbf{Pt,P}}$) to 2.25(4) Å ($\mathbf{3}^{\mathbf{Pt,P}}$). This effect is also observed for both arsenide analogues $\mathbf{3}^{\mathbf{Pd,As}}$ (Δd = −0.12 Å) and $\mathbf{3}^{\mathbf{Pt,As}}$ (Δd = −0.21 Å). Based on Pyykkö's covalent radii, the M–Pn bonds lengths are in the range between single and double bonds.[43] This is consistent with our earlier reports on the analogous triplet metallonitrenes [$d_{Pd-N}(\mathbf{3}^{\mathbf{Pd,N}})$ = 1.92(2) Å, $d_{Pt-N}(\mathbf{3}^{\mathbf{Pt,N}})$ = 1.874(11) Å], which were ultimately determined to exhibit M–N single bond character.[27] DFT optimized geometries reproduced all M–Pn bond lengths within experimental errors (Table S13).

Electronic Structure Characterization of the Metallopnictinidenes. To identify systematic trends in electronic structure, we first turn to electronic absorption spectroscopy. We limit the discussion in the following to the platinum pnictinidenes; all data obtained for the palladium congeners are presented as Supporting Information. The precursor complexes were photolyzed to the corresponding pnictinidenes $\mathbf{3}^{\mathbf{Pt,Pn}}$ in frozen 2-methyltetrahydrofuran glass at 77 K to suppress bimolecular coupling. In all cases, irradiation results in the evolution of qualitatively similar spectra with four new absorption features in the visible region that exhibit characteristic shifts along the pnictide series (Figure 6). Upon thawing, these spectroscopic signatures rapidly decay due to Pn–Pn coupling, which is highly exergonic (cf. DFT results in Table

https://doi.org/10.1021/jacs.4c16830
J. Am. Chem. Soc. 2025, 147, 5330–5339

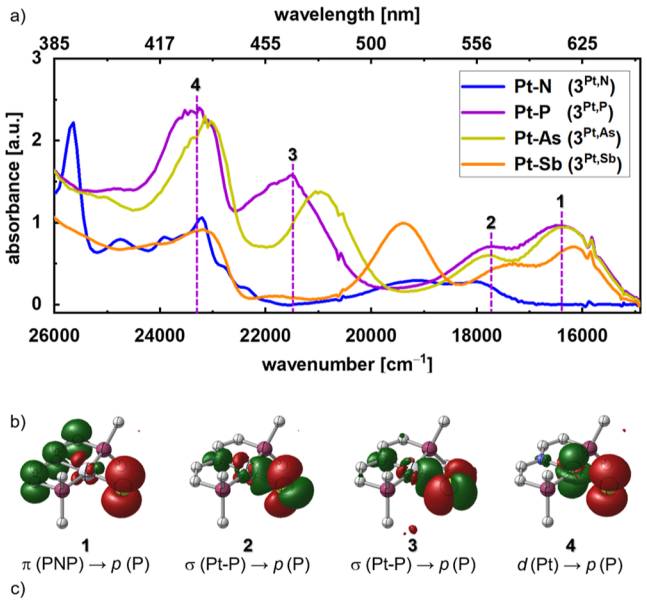

c)

	Transition	Experimental (TDDFT) [cm^{-1}]			
		$3^{Pt,N}$	$3^{Pt,P}$	$3^{Pt,As}$	$3^{Pt,Sb}$
1	π (PNP) → p (Pn)	18 000 (19 900)	16 500 (16 800)	16 400 (16 300)	16 200 (15 600)
2	σ (Pt-Pn) → p (Pn)	19 200 (20 700)	17 700 (18 800)	17 800 (18 00)	17 500 (16 400)
3	σ (Pt-Pn) → p (Pn)	23 200 (25 900)	21 500 (23 100)	21 000 (21 800)	19 400 (19 700)
4	d(Pt) → p (Pn)	25 600 (28 200)	23 400 (24 300)	23 100 (23 400)	23 200 (22 900)

Figure 6. (a) UV/vis spectra of the metallopnictinidenes $\mathbf{3}^{Pt,Pn}$ after photolysis of the precursors $\mathbf{1}^{Pt,Pn}$ in frozen MeTHF at 77 K. (b) DFT computed transition difference densities (green: electron depopulation, red: electron population) of the respective transitions of $\mathbf{3}^{Pt,P}$. (c) Assignment of the experimental data for the series $\mathbf{3}^{Pt,Pn}$ (Pn = N−Sb) with TD-DFT computed data in parentheses.

S7). Notably, significantly higher thermal stability in solution was reported for the nitrene analogue. Decay of the UV/vis and NMR signatures of $\mathbf{3}^{Pt,N}$ was observed at temperatures above approximately 203 K.[27,38] We tentatively attribute the higher solution lifetime of the nitrene to the significantly shorter Pt−N bond [1.874(11) Å] compared with the heavier homologues [e.g., Pt−P: 2.25(4) Å). In consequence, diffusion-controlled coupling is more efficiently shielded by the ^{t}Bu groups around the nitrene.

The similarity of the electronic absorption spectra along the pnictinidene series (Pn = N−Sb) suggests analogous electronic structures. Indeed, the quantum chemical analysis indicates far reaching similarities. CASSCF(18,11)/NEVPT2 computations revealed triplet ground states with negligible multireference character for all pnictinidenes ($|p_x^1 p_y^1\rangle$ determinantal representation in the pnictogen p_π atomic orbital space with z-axis alignment of the M−Pn bond). The lowest singlet states exhibit pronounced multireference character [$|p_x^2 p_y^0\rangle - \lambda|p_x^0 p_y^2\rangle$] and are energetically well separated from the ground state, yet with significantly smaller vertical singlet/triplet gaps (=$\Delta E_S - \Delta E_T$) for the heavier pnictinidenes M−Pn (Pn = P−Bi: 12−14 kcal·mol^{-1}) than for the nitrene analogues (21−23 kcal·mol^{-1}, cf. Table S17). In all cases, the second exited state, with $|p_x^\uparrow p_y^\downarrow\rangle - |p_x^\downarrow p_y^\uparrow\rangle$ singlet character throughout, is only 2−3 kcal·mol^{-1} higher in energy. By and large, state ordering of the metallopnictinidenes thus reflects that of imidogen ($^3\Sigma^-$, $^1\Delta$, and $^1\Sigma^+$), or simple pnictinidenes like Me−Pn ($^3A_2$, ^1E, and $^1A_1$),[5,46] which is in line with the Salem-Rowland bonding model for heterosymmetric diradicals.[3a]

NBO analyses of the triplet ground states revealed M−Pn single bonding and predominant localization of the unpaired electrons in two orthogonal atomic p_{Pn} orbitals (Figure 7a). In

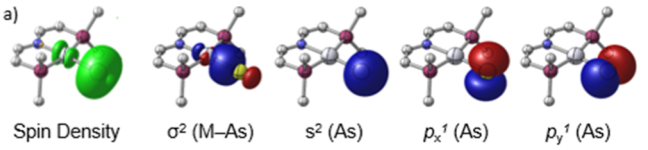

b)

Pn	NPA Charges		NPA Spin Population	
	$3^{Pd,Pn}$	$3^{Pt,Pn}$	$3^{Pd,Pn}$	$3^{Pt,Pn}$
N [26]	−0.46	−0.52	1.91	1.81
P	−0.25	−0.27	1.88	1.83
As	−0.22	−0.23	1.90	1.86
Sb	−0.14	−0.15	1.93	1.90
Bi	−0.12	−0.12	1.95	1.92

Figure 7. (a) DFT computed spin density of $\mathbf{3}^{Pt,As}$ and selected NLMOs (cf. Supporting Information for other pnictinidenes). The doubly occupied NLMOs are obtained by averaging over the α and β spin orbitals. (b) NPA charges and spin populations of the pnictide ligands of $\mathbf{3}^{M,Pn}$.

consequence, the spin populations show toroidal distributions around the pnictogen atoms with little delocalization onto the metal ions (5−14%). In fact, spin localization at the Pn atom further increases along the pnictide series with almost complete localization in case of Sb and Bi (Figure 7b). Natural population analysis (NPA) also revealed significantly less negative NPA charges for the heavier pnictide ligands (Figure 7b), reflecting Allen's spectroscopic electronegativity scale along the pnictogen series [configuration energies in Pauling units: 3.07 (N), 2.25 (P), 2.21 (As), 1.98 (Sb)].[47]

More detailed interpretation of the electronic absorption spectra was carried out by aid of TD-DFT simulations for the triplet pnictinidenes. The experimental data was nicely reproduced, using the B3LYP functional and a ZORA scalar-relativistic Hamiltonian along with the corresponding relativistically recontracted basis sets (Figure 6, cf. Supporting Information for details). Notably, the character of the four main transitions in the visible region does not change along the series, allowing for direct comparison. The lowest excitation with dominant π(PNP) → p(Pn) ligand-to-ligand charge transfer character (Figure 6b, **1**) proved particularly instructive, as the pincer-based donor orbital energy is system independent. Thus, the red-shift of this transition for all heavier pnictide complexes with respect to the nitrene ($\Delta\tilde{\nu} \approx$ 1700 cm^{-1}) directly indicates a significant lowering of their SOMO energies.

Magnetic Characterization of the Metallopnictinidenes. Relativistic effects were evaluated by examination of the magnetic properties with *in situ* SQUID magnetometry. Continuous photolysis of solid $\mathbf{1}^{Pd,P}$, $\mathbf{1}^{Pd,As}$, $\mathbf{1}^{Pt,P}$, and $\mathbf{1}^{Pt,As}$ at 5 K results in constant rise of the magnetization (Figures S52−S59) due to formation of the respective paramagnetic

https://doi.org/10.1021/jacs.4c16830
J. Am. Chem. Soc. 2025, 147, 5330−5339

pnictinidene photoproducts. The $\chi_m T$ products of $\mathbf{3}^{\mathbf{Pd,P}}$, $\mathbf{3}^{\mathbf{Pd,As}}$, $\mathbf{3}^{\mathbf{Pt,P}}$, and $\mathbf{3}^{\mathbf{Pt,As}}$ (Figure 8a) rise with temperature and sharply

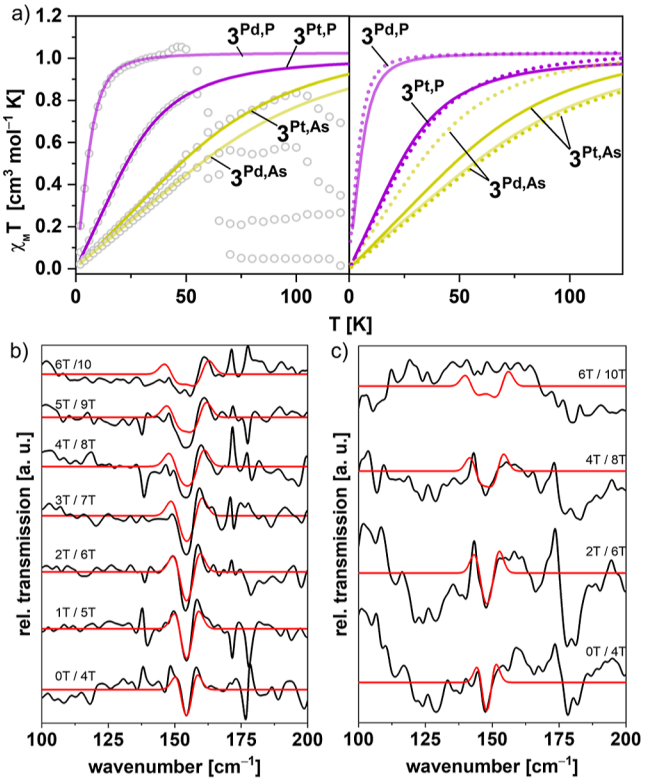

d)

	[M(Pn)(PNP)]	D_{exp} [cm^{-1}]	D_{comp} [cm^{-1}]
Pd	N ($\mathbf{3}^{\mathbf{Pd,N}}$) [27b]	9	6
	P ($\mathbf{3}^{\mathbf{Pd,P}}$)	15	12
	As ($\mathbf{3}^{\mathbf{Pd,As}}$)	169 (154.5(3))	95
	Sb ($\mathbf{3}^{\mathbf{Pd,Sb}}$)	n.d.	425
	Bi ($\mathbf{3}^{\mathbf{Pd,Bi}}$)	n.d.	2240
Pt	N ($\mathbf{3}^{\mathbf{Pt,N}}$) [27a]	85	80
	P ($\mathbf{3}^{\mathbf{Pt,P}}$)	63	70
	As ($\mathbf{3}^{\mathbf{Pt,As}}$)	143 (148.0(5))	172
	Sb ($\mathbf{3}^{\mathbf{Pt,Sb}}$)	n.d.	481
	Bi ($\mathbf{3}^{\mathbf{Pt,Bi}}$)	n.d.	2161

Figure 8. (a) SQUID magnetometric characterization of *in situ* formed $\mathbf{3}^{\mathbf{Pd,P}}$, $\mathbf{3}^{\mathbf{Pd,As}}$ and $\mathbf{3}^{\mathbf{Pt,P}}$, $\mathbf{3}^{\mathbf{Pt,As}}$; left: experimental (circles) and simulated (colored lines) $\chi_m T$ vs T data; right: comparison of simulated (colored lines) and *ab initio* computed (dotted lines) $\chi_m T$ vs T data. (b) THz-EPR data (black lines) and numerical simulations (red lines; cf. Supporting Information for details) of $\mathbf{3}^{\mathbf{Pd,As}}$. (c) THz-EPR data (black lines) and numerical simulations (red lines; cf. Supporting Information for details) of $\mathbf{3}^{\mathbf{Pt,As}}$. (d) Comparison of axial zero-field splitting parameters D from SQUID magnetometry and THz-EPR (in paratheses) with *ab initio* computed values (cf. Supporting Information for details).

drop beyond 50−100 K, indicating sample decay. The apparently higher sample stability during single crystal photolysis experiments (100 K), might be caused by lower CO gas mobility within the larger crystals, but ultimately remains unknown. In consequence, the accessible temperature ranges for magnetic characterization were markedly smaller than for the nitrogen analogues. Nevertheless, pronounced deviation from purely temperature independent paramagnetism allowed for reliably fitting the conversion-normalized magnetic data of $\mathbf{3}^{\mathbf{Pd,P}}$, $\mathbf{3}^{\mathbf{Pt,P}}$, and $\mathbf{3}^{\mathbf{Pt,As}}$ to a ZFS spin-Hamilitonian (sH) for spin triplet ground states (S = 1) and isotropic g-factors fixed to g = 2 (Figure 8a). The low magnetic moment of the sample after photolysis of $\mathbf{1}^{\mathbf{Pt,Sb}}$ prohibited meaningful simulation of the magnetic data.

Due to the limited temperature range of the magnetic data, variable field (0−10 T) *in situ* THz-EPR spectroscopy was used to determine the ZFS of *in situ* photogenerated $\mathbf{3}^{\mathbf{Pd,As}}$ and $\mathbf{3}^{\mathbf{Pt,As}}$ (λ_{exc} = 532 nm) directly from the transitions between the magnetic sublevels at 5 K. Notably, fitting of the field-dependent data to a ZFS-sH (Figure 8b,c) gave axial ZFS parameters D that are in nice agreement with the SQUID simulations (Figure 8d). Furthermore, the data confirmed g values close to 2 and negligible rhombicity in the ZFS.

The axial ZFS parameters of both metallophoshinidenes are close to those of the respective nitrene analogues but vary significantly with the nature of the metal substituent. Furthermore, the values are markedly higher than the ZFS that was calculated by Michl and co-workers for simple organic nitrenes and phosphinidenes, like Me−Pn [Pn = N, P; D/cm^{-1} = 1.8 (N), 3.5 (P)].[6b] This finding supports the notion that magnetic sublevel splitting of the lighter pnictinidenes (N, P) is dominated by metal-induced spin−orbit coupling (SOC) of the ground and excited states. Notably, the ZFS slightly drops from $\mathbf{3}^{\mathbf{Pt,N}}$ to the heavier $\mathbf{3}^{\mathbf{Pt,P}}$ (Figure 8d), albeit the excited states of the phosphinidene are significantly lower in energy (see above). We tentatively attribute this observation to overcompensation from decreased Pt−P orbital overlap and, thus, lower effective SOC.

In turn, the arsinidenes exhibit substantially higher ZFS parameters, while the difference between the two transition metal platforms almost vanishes. We note in passing, that the ZFS parameters of the metalloarsinidenes are closer to the value computed for Me−As (D/cm^{-1} = 86.5),[6b] as compared with the phosphorus analogues. Quantum-chemical expansion of the magnetic data toward the heaviest pnictinidenes (Sb, Bi), which were so far not accessible experimentally, predicts further rising D values and ultimately negligible differences between the two transition metal platforms for $\mathbf{3}^{\mathbf{Pd,Bi}}$ and $\mathbf{3}^{\mathbf{Pt,Bi}}$ (Figure 8d). Note that the axial ZFS computed for the metallobismuthinidenes is of similar magnitude as the energetic separation that Neese and Cornella found for the nonmagnetic ground state of their isolable triplet bismuthinidene (D > 5400 cm^{-1}; Figure 1b). Thus, for the arsinidene and beyond the splitting of the magnetic microstates is dominated by pnictogen-induced SOC effects. This interpretation is in line with exclusive localization of the spin orbitals at the pnictide ligand, as supported by the NBO analysis.

CONCLUSIONS

In continuation of our report about the meatllonitrenes [M(N)(PNP)] (M = Pd, Pt),[27] we have characterized the heavier metallopnictinidenes [M(Pn)(PNP)] (Pn = P−Sb) as transient precursors to bimolecular pnictide coupling. In addition to the common pnictaenthynolate precursors for the introduction of atomic P and As ligands, the parent antimonide, SbH_2^-, proved effective for stibinidene generation upon UV-induced H_2 elimination. In analogy to the metallonitrenes, the spectroscopic, magnetic, and computational analysis confirmed predominantly pnictide-centered diradicals with triplet ground states. Beyond N and P, excited state admixture through spin−orbit coupling is predominantly induced by the heavy pnictide atom.

Importantly, the electronic structure examinations revealed some trends of the heavier pnictides versus their nitrogen

https://doi.org/10.1021/jacs.4c16830
J. Am. Chem. Soc. 2025, 147, 5330−5339

analogues with potential relevance for chemical reactivity. First, the lowest singlet excited states are all at significantly lower energy. Thus, reactions that require crossover onto the singlet surface might proceed with markedly smaller electronic reorganization energies. Note that Bertrand's group showed that singlet phosphinidenes exhibit distinctly electrophilic reactivity.[19b] Furthermore, the lowest SOMOs of the heavier pnictinidenes feature lower energies than those of the nitrenes. This observation also suggests increased electrophilicity in radical reactions, which contrasts with the distinct nucleophilicity of the metallonitrenes.[28,38] Future studies will focus on the exploration of these predictions for chemical synthesis.

■ ASSOCIATED CONTENT

Supporting Information

The Supporting Information is available free of charge at https://pubs.acs.org/doi/10.1021/jacs.4c16830.

Experimental procedures, spectroscopic data and computational details for the discussed structures (PDF)

Cartesian coordinates (TXT)

Accession Codes

CCDC 2383559, 2383512, 2383555, 2387991, 2383521, 2383513, 2383556, 2383519, 2387995, 2381476, 2381475, 2381478 and 2381477 contain the supplementary crystallographic data for this paper. These data can be obtained free of charge via www.ccdc.cam.ac.uk/data_request/cif, or by emailing data_request@ccdc.cam.ac.uk, or by contacting The Cambridge Crystallographic Data Centre, 12 Union Road, Cambridge CB21EZ, UK; fax: +44 1223 336033.

■ AUTHOR INFORMATION

Corresponding Authors

Carsten von Hänisch − *Fachbereich Chemie, Philipps-Universität Marburg, 35043 Marburg, Germany*; Email: haenisch@chemie.uni-marburg.de

Max C. Holthausen − *Institut für Anorganische und Analytische Chemie Goethe-Universität, 60438 Frankfurt am Main, Germany*; orcid.org/0000-0001-7283-8329; Email: max.holthausen@chemie.uni-frankfurt.de

David C. Powers − *Department of Chemistry, Texas A&M University, College Station, Texas 77843, United States*; orcid.org/0000-0003-3717-2001; Email: powers@chem.tamu.edu

Alexander Schnegg − *EPR Research Group, MPI for Chemical Energy Conversion, 45470 Mülheim Ruhr, Germany*; orcid.org/0000-0002-2362-0638; Email: alexander.schnegg@cec.mpg.de

Sven Schneider − *Institut für Anorganische Chemie and International Center for Advanced Studies of Energy Conversion, Georg-August-Universität Göttingen, 37077 Göttingen, Germany*; orcid.org/0000-0002-8432-7830; Email: sven.schneider@chemie.uni-goettingen.de

Authors

Marc C. Neben − *Institut für Anorganische Chemie and International Center for Advanced Studies of Energy Conversion, Georg-August-Universität Göttingen, 37077 Göttingen, Germany*

Nils Wegerich − *Institut für Anorganische und Analytische Chemie Goethe-Universität, 60438 Frankfurt am Main, Germany*

Tarek A. Al Said − *Helmholtz-Zentrum Berlin für Materialien und Energie GmbH, 14109 Berlin, Germany; EPR Research Group, MPI for Chemical Energy Conversion, 45470 Mülheim Ruhr, Germany*; orcid.org/0000-0002-9057-5451

Richard R. Thompson − *Department of Chemistry, University of Idaho, Moscow, Idaho 83844, United States*; orcid.org/0000-0002-2181-9846

Serhiy Demeshko − *Institut für Anorganische Chemie and International Center for Advanced Studies of Energy Conversion, Georg-August-Universität Göttingen, 37077 Göttingen, Germany*

Kevin Dollberg − *Fachbereich Chemie, Philipps-Universität Marburg, 35043 Marburg, Germany*

Igor Tkach − *RG ESR Spectroscopy, Max Planck Institute for Multidisciplinary Sciences, 37077 Göttingen, Germany*

Gerard P. Van Trieste, III − *Department of Chemistry, Texas A&M University, College Station, Texas 77843, United States*

Hendrik Verplancke − *Institut für Anorganische und Analytische Chemie Goethe-Universität, 60438 Frankfurt am Main, Germany*

Complete contact information is available at: https://pubs.acs.org/10.1021/jacs.4c16830

Author Contributions

[&]M.C.N. and N.W. equally contributed to this work.

Notes

The authors declare no competing financial interest.

■ ACKNOWLEDGMENTS

S. Sch. thanks Dr. C. Hering-Junghans for discussion. Dr. S. Dechert and Dr. M. Otte are acknowledged for the determination of X-ray diffraction data, C. Siebert for NMR measurements, Dr. J. Sun for contributions to chemical synthesis and T. Schmidt-Räntsch for UV/vis measurements. The German Research Foundation (DFG) is acknowledged for funding (S. Sch. Priority Program 2102, Grant SCHN950/6-2); the U.S. Department of Energy (DOE), Office of Science, Office of Basic Energy Sciences, Catalysis Program (DE-SC0024121), the Welch Foundation (A-1907), and the Alexander von Humboldt Foundation for support to D.C.P. *In situ* crystallographic experiments were attempted at NSF's ChemMatCARS Sector 15, which is principally supported by the Divisions of Chemistry (CHE) and Materials Research (DMR), NSF, under Grant NSF/CHE-2335833. Use of the Advanced Photon Source, an Office of Science User Facility operated for the U.S. DOE Office of Science by Argonne National Laboratory, was supported by the U.S. DOE under Contract DE-AC02-06CH11357. We thank the Helmholtz-Zentrum Berlin für Materialien und Energie (HZB) for the allocation of synchrotron radiation beamtime at BESSY II (232-12175ST) and acknowledge financial support by HZB. Dr. Karsten Holldack is acknowledged for his advice and assistance to enable the light-induced THz-EPR experiments. Computing resources and excellent service were provided by the NHR Center NHR@SW and the Centre for Scientific Computing (CSC) at Goethe-University Frankfurt.

■ REFERENCES

(1) (a) Falvey, D. E.; Gudmundsdottir, A. D. *Nitrenes and Nitrenium Ions*, 1st ed.; J. Wiley & Sons, 2013. (b) Albini, A.; Fagnioni, M.

Photogeneration of Carbenes and Nitrenes. In *Photochemically-Generated Intermediates in Synthesis*; J. Wiley & Sons, 2013; pp 302−327.
(2) (a) Gritsan, N. P.; Platz, M. S. Kinetics, Spectroscopy, and Computational Chemistry of Arylnitrenes. *Chem. Rev.* **2006**, *106*, 3844−3867. (b) Wentrup, C. Flash Vacuum Pyrolysis of Azides, Triazoles, and Tetrazoles. *Chem. Rev.* **2017**, *117*, 4562−4623. (c) Wentrup, C. Carbenes and Nitrenes: Recent Developments in Fundamental Chemistry. *Angew. Chem., Int. Ed.* **2018**, *57*, 11508−11521.
(3) (a) Salem, L.; Rowland, C. The Electronic Properties of Diradicals. *Angew. Chem. Int. Ed.* **1972**, *11*, 92−111. (b) Bonačić-Koutecký, V.; Koutecký, J.; Michl, J. Neutral and Charged Biradicals, Zwitterions, Funnels in S_1, and Proton Translocation: Their Role in Photochemistry, Photophysics, and Vision. *Angew. Chem., Int. Ed.* **1987**, *26*, 170−189.
(4) (a) Huo, W. M. Valence Excited States of NH and CH and Theoretical Transition Probabilities. *J. Chem. Phys.* **1968**, *49*, 1482−1492. (b) O'Neil, S. V.; Schaefer, H. F. Configuration Interaction Study of the $X^3\Sigma^-$, $a^1\Delta$, and $b^1\Sigma^+$ States of NH. *J. Chem. Phys.* **1971**, *55*, 394−401.
(5) Yarkony, D. R.; Schaefer, I. I. I.; Rothenburg, S. X. $^3A_2$, a ^1E, and b $^1A_1$ Electronic States of Methylnitrene. *J. Am. Chem. Soc.* **1974**, *96*, 5974−5977.
(6) (a) Smolinsky, G.; Wasserman, E.; Yager, W. A. The E.P.R. of Ground State Triplet Nitrenes. *J. Am. Chem. Soc.* **1962**, *84*, 3220−3221. (b) Havlas, Z.; Kývala, M.; Michl, J. Spin-Orbit Coupling in Biradicals. 4. Zero-Field Splitting in Triplet Nitrenes, Phosphinidenes, and Arsinidenes. *Collect. Czech. Chem. Commun.* **2003**, *68*, 2335−2343.
(7) (a) Janssen, M.; Frederichs, T.; Olaru, M.; Lork, E.; Hupf, E.; Beckmann, J. Synthesis of a Stable Crystalline Nitrene. *Science* **2024**, *385*, 318−321. (b) Wang, D.; Chen, W.; Chen, H.; Chen, Y.; Ye, S.; Tan, G. Isolation and characterization of a triplet nitrene. *Nat. Chem.* **2025**, *17*, 38.
(8) Vyas, S.; Winter, A. H.; Hadad, C. M. Theory and Computation in the Study of Nitrenes and their Excited-State Photoprecursors. In *Nitrenes and Nitrenium Ions*; J. Wiley & Sons, 2013.
(9) Dielmann, F.; Back, O.; Henry-Ellinger, M.; Jerabek, P.; Frenking, G.; Bertrand, G. A Crystalline Singlet Phosphinonitrene: A Nitrogen Atom-Transfer Agent. *Science* **2012**, *337*, 1526−1528.
(10) Lu, B.; Zeng, X. Phosphinidenes: Fundamental Properties and Reactivity. *Chem.—Eur. J.* **2024**, *30*, No. e202303283.
(11) (a) Minh Tho, N.; McGinn, M. A.; Hegarty, A. F. R_2PCR: λ^3-Phosphinocarbene vs λ^5-Phosphaacetylene. Theoretical Study of the CH_3P Isomers. *Inorg. Chem.* **1986**, *25*, 2185−2190. (b) Kim, S.-J.; Hamilton, T. P.; Schaefer, H. F., III; H, F. Methylphosphinidene (CH_3P) and Its Rearrangement to Phosphaethylene (CH_2PH): Toward the Observation of Ground-State Triplet CH_3P. *J. Phys. Chem.* **1993**, *97*, 1872−1877. (c) Nguyen, M. T.; Creve, S.; Verquickenborne, L. G. Properties of Phosphorus Compounds by Density Functional Theory: CH_3P Species as a Test Case. *J. Chem. Phys.* **1996**, *105*, 1922−1932.
(12) Mukhopadhyay, D. P.; Gerlach, M.; Hartweg, S.; Fischer, I.; Loison, J.-C. Photoelectron Spectroscopy of Low Valent Organophosphorus Compounds, P-CH_3,H-P = CH_2 and P = CH_2. *Phys. Chem. Chem. Phys.* **2022**, *24*, 10993−10999.
(13) (a) Li, X.; Weissman, S. I.; Lin, T.-S.; Gaspar, P. P.; Cowley, A. H.; Smirnov, A. I. Observation of a Triplet Phosphinidene by ESR Spectroscopy. *J. Am. Chem. Soc.* **1994**, *116*, 7899−7900. (b) Akimov, A. V.; Ganushevich, Y. S.; Korchagin, D. V.; Miluykov, V. A.; Misochko, E. Y. The EPR Spectrum of Triplet Mesitylphosphinidene: Reassignment and New Assignment. *Angew. Chem., Int. Ed.* **2017**, *56*, 7944−7947.
(14) (a) Bucher, G.; Borst, M. L. G.; Ehlers, A. W.; Lammertsma, K.; Ceola, S.; Huber, M.; Grote, D.; Sander, W. Infrared, UV/Vis, and W-band EPR Spectroscopic Characterization and Photochemistry of Triplet Mesitylphosphinidene. *Angew. Chem. Int. Ed.* **2005**, *44*, 3289−3293. (b) Mardyukov, A.; Niedek, D.; Schreiner, P. R. Preparation and Characterization of Parent Phenylphosphinidene and Its Oxidation to Phenyldioxophosphorane: The Elusive Phosphorus Analogue of Nitrobenzene. *J. Am. Chem. Soc.* **2017**, *139*, 5019−5022. (c) Qian, W.; Schreiner, P. R.; Mardyukov, A. Triplet Phenylarsinidene and Its Oxidation to Dioxophenylarsine. *J. Am. Chem. Soc.* **2023**, *145*, 12755−12759. (d) Qian, W.; Schreiner, P. R.; Mardyukov, A. Preparation and Photochemistry of Parent Triplet Vinylarsinidene. *J. Am. Chem. Soc.* **2024**, *146*, 930−935.
(15) Mukhopadhyay, D. P.; Schleier, D.; Wirsing, S.; Ramler, J.; Kaiser, D.; Reusch, E.; Hemberger, P.; Preitschopf, T.; Krummenacher, I.; Engels, B.; Fischer, I.; Lichtenberg, C. Methylbismuth: an Organometallic Bismuthinidene Biradical. *Chem. Sci.* **2020**, *11*, 7562−7568.
(16) Bi: (a) Pang, Y.; Nöthling, N.; Leutzsch, M.; Kang, L.; Bill, E.; van Gastel, M.; Reijerse, E.; Goddard, R.; Wagner, L.; SantaLucia, D.; DeBeer, S.; Neese, F.; Cornella, J. Synthesis and Isolation of a Triplet Bismuthinidene with a Quenched Magnetic Response. *Science* **2023**, *380*, 1043−1048. (b) Wu, M.; Chen, W.; Wang, D.; Chen, Y.; Ye, S.; Tan, G. Triplet Bismuthinidenes Featuring Unprecedented Giant and Positive Zero Field Splittings. *Natl. Sci. Rev.* **2023**, *10*, nwad169.
(17) Wu, M.; Li, H.; Chen, W.; Wang, D.; He, Y.; Xu, L.; Ye, S.; Tan, G. A Triplet Stibinidene. *Chem.* **2023**, *9*, 2573−2584.
(18) Chen, Y.; Su, P.; Wang, D.; Ke, Z.; Tan, G. Molecular-strain Induced Phosphinidene Reactivity of a Phosphanorcaradiene. *Nat. Commun.* **2024**, *15*, 4579.
(19) (a) Liu, L.; Ruiz, D. A.; Munz, D.; Bertrand, G. A Singlet Phosphinidene Stable at Room Temperature. *Chem* **2016**, *1*, 147−153. (b) Hansmann, M. M.; Jazzar, R.; Bertrand, G. Singlet (Phosphino)phosphinidenes are Electrophilic. *J. Am. Chem. Soc.* **2016**, *138*, 8356−8359.
(20) Al Said, T.; Spinnato, D.; Holldack, K.; Neese, F.; Cornella, J.; Schnegg, A. Direct Determination of a Giant Zero-Field Splitting of 5422 cm^{-1} in a Triplet Organobismuthinidene by Infrared Electron Paramagnetic Resonance. *J. Am. Chem. Soc.* **2025**, *147*, 84−87.
(21) (a) Moon, H. W.; Cornella, J. Bismuth Redox Catalysis: An Emerging Main-Group Platform for Organic Synthesis. *ACS Catal.* **2022**, *12*, 1382−1393. (b) Oberdorf, K.; Lichtenberg, C. Small Molecule Activation by Well-defined Compounds of Heavy p-block Elements. *Chem. Commun.* **2023**, *59*, 8043−8058. (c) Mato, M.; Cornella, J. Bismuth in Radical Chemistry and Catalysis. *Angew. Chem., Int. Ed.* **2024**, *63*, No. e202315046.
(22) (a) Fritz, G.; Vaahs, T.; Fleischer, H.; Matern, E. $^tBu_2P$-P = PBr^tBu_2·LiBr und die Bildung von tBu_2P-P. *Angew. Chem.* **1989**, *101*, 324−325. (b) Li, X.; Lei, D.; Chiang, M. Y.; Gaspar, P. P. General Approaches to Phosphinidenes via Retroadditions. *J. Am. Chem. Soc.* **1992**, *114*, 8526−8531. (c) Velian, A.; Cummins, C. C. Facile Synthesis of Dibenzo-7λ^3-phosphanorbornadiene Derivatives Using Magnesium Anthracene. *J. Am. Chem. Soc.* **2012**, *134*, 13978−13981.
(23) (a) Becker, G.; Schwarz, W.; Seidler, N.; Westernhausen, M. Lithoxy-methylidenphosphan·DME und -methylidinphosphan·2 DME - Synthese und Struktur. *Z. Anorg. Allg. Chem.* **1992**, *612*, 77−82. (b) Puschmann, F. F.; Stein, D.; Heift, D.; Hendriksen, C.; Gal, Z. A.; Grützmacher, H.-F.; Grützmacher, H. Phosphination of Carbon Monoxide: A Simple Synthesis of Sodium Phosphaethynolate (NaOCP). *Angew. Chem., Int. Ed.* **2011**, *50*, 8420−8423. (c) Jupp, A. R.; Goicoechea, J. M. The 2-Phosphaethynolate Anion: A Convenient Synthesis and [2 + 2] Cycloaddition Chemistry. *Angew. Chem., Int. Ed.* **2013**, *52*, 10064−10067. (d) Hinz, A.; Goicoechea, J. M. The 2-Arsaethynolate Anion: Synthesis and Reactivity Towards Heteroallenes. *Angew. Chem. Int. Ed.* **2016**, *55*, 8536−8541.
(24) Goicoechea, J. M.; Grützmacher, H. The Chemistry of the 2-Phosphaethynolate Anion. *Angew. Chem., Int. Ed.* **2018**, *57*, 16968−16994.
(25) (a) Liu, L.; Ruiz, D. A.; Dahcheh, F.; Bertrand, G.; Suter, R.; Tondreau, A. M.; Grützmacher, H. Isolation of Au-, Co-η^1PCO and Cu-η^2PCO Complexes, Conversion of an Ir-η^1PCO Complex Into a Dimetalladiphosphene, and an Interaction-free PCO Anion. *Chem. Sci.* **2016**, *7*, 2335−2341. (b) Grant, L. N.; Pinter, B.; Manor, B. C.; Suter, R.; Grützmacher, H.; Mindiola, D. J. A Planar Ti_2P_2 Core

https://doi.org/10.1021/jacs.4c16830
J. Am. Chem. Soc. 2025, 147, 5330−5339

Assembled by Reductive Decarbonylation of $^{-}$O−C≡P and P−P Radical Coupling. *Chem.—Eur. J.* **2017**, *23*, 6272−6276. (c) Joost, M.; Transue, W. J.; Cummins, C. C. Terminal Tungsten Pnictide Complex Formation Through Pnictaethynolate Decarbonylation. *Chem. Commun.* **2017**, *53*, 10731−10733. (d) Hierlmeier, G.; Hinz, A.; Wolf, R.; Goicoechea, J. M. Synthesis and Reactivity of Nickel-Stabilised μ^2:η^2,η^2-P_2, As_2 and PAs Units. *Angew. Chem., Int. Ed.* **2018**, *57*, 431−436. (e) Abbenseth, J.; Diefenbach, M.; Hinz, A.; Alig, L.; Würtele, C.; Goicoechea, J. M.; Holthausen, M.; Schneider, S. Oxidative Coupling of Terminal Rhenium Pnictide Complexes. *Angew. Chem., Int. Ed.* **2019**, *58*, 10966−10970. (f) Magnall, R.; Balázs, G.; Lu, E.; Kern, M.; van Slageren, J.; Tuna, F.; Wooles, A. J.; Scheer, M.; Liddle, S. T. Photolytic and Reductive Activations of 2-Arsaethynolate in a Uranium-Triamidoamine Complex: Decarbonylative Arsenic-Group Transfer Reactions and Trapping of a Highly Bent and Reduced Form. *Chem.—Eur. J.* **2019**, *25*, 14246−14252.

(26) Thompson, R. R.; Figgins, M. T.; Wannipurage, D. C.; Rentiera-Gomez, A.; Gogoi, A. R.; Telser, J.; Tierney, D. L.; Neben, M. C.; Demeshko, S.; Gutierrez, O.; Powers, D. C. P-P Coupling with and without Terminal Metal-Phosphorous Intermediates. *J. Am. Chem. Soc.* DOI: 10.1021/jacs.4c16833.

(27) (a) Sun, J.; Abbenseth, J.; Verplancke, H.; Diefenbach, M.; de Bruin, B.; Hunger, D.; Würtele, C.; van Slageren, J.; Holthausen, M. C.; Schneider, S. A Platinum(II) Metallonitrene with a Triplet Ground State. *Nat. Chem.* **2020**, *12*, 1054−1059. (b) Schmidt-Räntsch, T.; Verplancke, H.; Lienert, J. N.; Demeshko, S.; Otte, M.; Van Trieste, G. P.; Reid, K. A.; Reibenspies, J. H.; Powers, D. C.; Holthausen, M. C.; Schneider, S. Nitrogen Atom Transfer Catalysis by Metallonitrene C−H Insertion: Photocatalytic Amidation of Aldehydes. *Angew. Chem., Int. Ed.* **2022**, *61*, No. e202115626.

(28) Sun, J.; Verplancke, H.; Schweizer, J. I.; Diefenbach, M.; Würtele, C.; Otte, M.; Tkach, I.; Herwig, C.; Limberg, C.; Demeshko, S.; Holthausen, M. C.; Schneider, S. Stabilizing P = P: P_2^{2-}, $P_2^{\cdot-}$, and P_2^{0} as Bridging Ligands. *Chem* **2021**, *7*, 1952−1962.

(29) Kaupp, M. Chemical Bonding of Main-Group Elements. In *The Chemical Bond: Chemical Bonding Across the Periodic Table*; Wiley VCH, 2014; pp 1−24.

(30) Lu, Y.; Wang, H.; Xie, Y.; Liu, H.; Schaefer, H. F. The Cyanate and 2-Phosphaethynolate Anion Congeners ECO^- (E = N, P, As, Sb, Bi): Prelude to Experimental Characterization. *Inorg. Chem.* **2014**, *53*, 6252−6256.

(31) Du, J.; Dollberg, K.; Seed, J. A.; Wooles, A. J.; von Hänisch, C.; Liddle, S. T. Thorium(IV)-Antimony Complexes Exhibiting Single, Double, and Triple Polar Covalent Metal-Metal Bonds. *Nat. Chem.* **2024**, *16*, 780−790.

(32) Dollberg, K.; Schneider, S.; Richter, R. M.; Dunaj, T.; von Hänisch, C. Synthesis and Application of Alkali Metal Antimonide - A New Approach to Antimony Chemistry. *Angew. Chem., Int. Ed.* **2022**, *61*, No. e202213098.

(33) Pang, Y.; Leutzsch, M.; Nöthling, N.; Cornella, J. Dihydrogen and Ethylene Activation by a Sterically Distorted Distibene. *Angew. Chem. Int. Ed.* **2023**, *62*, No. e202302071.

(34) Domenianni, L. I.; Bauer, M.; Schmidt-Räntsch, T.; Lindner, J.; Schneider, S.; Vöhringer, P. Photoinduced Metallonitrene Formation by N_2 Elimination from Azide Diradical Ligands. *Angew. Chem., Int. Ed.* **2023**, *62*, No. e202309618.

(35) (a) Breunig, H. J.; Müller, D. Tetraethyldibismuthane: A Dinuclear Bismuth Compound. *Angew. Chem., Int. Ed.* **1982**, *21*, 439−440. (b) Ashe, A. J.; Ludwig, E. G. A Reinvestigation of Paneth's Violet Compound. The Synthesis of Tetramethyldibismuthine. *Organometallics* **1982**, *1*, 1408−1410. (c) Breunig, H. J.; Müller, D. Tetraalkyldibismutane. *Z. Naturforsch.* **1983**, *38b*, 125−129. (d) Ashe, A. J.; Ludwig, E. G.; Oleksyszyn, J. Preparation and Properties of Dibismuthines. *Organometallics* **1983**, *2*, 1859−1866. (e) Breunig, H. J.; Müller, D. Spaltung von Triphenylbismutan mit Kalium. Bildung von Tetraphenyldibismutan und Diphenyl(ethyl)bismutan. *J. Organomet. Chem.* **1983**, *253*, C21−C22.

(36) Braunschweig, H.; Cogswell, P.; Schwab, K. Synthesis, Structure and Reactivity of Complexes Containing a Transition Metal-Bismuth Bond. *Coord. Chem. Rev.* **2011**, *255*, 101−117.

(37) Mather, G. G.; Pidcock, A.; Rapsey, G. J. N. Correlation of Nuclear Magnetic Resonance Coupling Constants with Transition Metal-Ligand Bond Lengths in Tertiary Phosphine Complexes. *J. Chem. Soc., Dalton Trans.* **1973**, 2095−2099.

(38) Schmidt-Räntsch, T.; Verplancke, H.; Kehl, A.; Sun, J.; Bennati, M.; Holthausen, M. C.; Schneider, S. C=C Dissociative Imination of Styrenes by a Photogenerated Metallonitrene. *JACS Au* **2024**, *4*, 3421−3426.

(39) (a) Weber, L. The Chemistry of Diphosphenes and Their Heavy Congeners: Synthesis, Structure, and Reactivity. *Chem. Rev.* **1992**, *92*, 1839−1906. (b) Fischer, R. C.; Power, P. P. π-Bonding and the Lone Pair Effect in Multiple Bonds Involving Heavier Main Group Elements: Developments in the New Millennium. *Chem. Rev.* **2010**, *110*, 3877−3923. (c) Weber, L.; Ebeler, F.; Ghadwal, R. S. Advances and Recent Trends in Dipnictenes Chemistry. *Coord. Chem. Rev.* **2022**, *461*, 214499.

(40) (a) Tokitoh, N.; Arai, Y.; Okazaki, R.; Nagase, S. Synthesis and Characterization of a Stable Dibismuthene: Evidence for a Bi-Bi Double Bond. *Science* **1997**, *277*, 78−80. (b) Vránová, I.; Alonso, M.; Lo, R.; Sedlál, R.; Jambor, R.; Ruzicka, A.; De Proft, F.; Hobza, P.; Dostál, L. From Dibismuthenes to Three- and Two-Coordinated Bismuthinidenes by Fine Ligand Tuning: Evidence for Aromatic BiC_3N Rings through a Combined Experimental and Theoretical Study. *Chem.—Eur. J.* **2015**, *21*, 16917. (c) Ho, L. P.; Tamm, M. Stabilization of a Bismuth-Bismuth Double Bond by Anionic N-heterocyclic Carbenes. *Dalton Trans.* **2021**, *50*, 1202−1205. (d) Schwamm, R. J.; Kilpatrick, A. F. R.; Coles, M. P. Catenated $(Bi)_n$ (n = 2, 3, 4) Complexes with Formally Monovalent Bismuth Centres. *Z. Anorg. Allg. Chem.* **2022**, *648*, No. e202200260. (e) Weinert, H. M.; Schulte, Y.; Gehlhaar, A.; Wölper, C.; Haberhauer, G.; Schulz, S. Metal-Coordinated Distibene and Dibismuthene Dications - Isoelectronic Analogues of Butadiene Dications. *Chem. Commun.* **2023**, *59*, 7755−7758. (f) Dabringhaus, P.; Molino, A.; Gilliard, R. J. Carbodiphosphorane-Activated Distibene and Dibismuthene Dications. *J. Am. Chem. Soc.* **2024**, *146*, 27186−27195.

(41) (a) Xu, L.; Bobev, S.; El-Bahraoui, J.; Sevov, S. C. A Naked Diatomic Molecule of Bismuth, $[Bi_2]^{2-}$, with a Short Bi-Bi Bond: Synthesis and Structure. *J. Am. Chem. Soc.* **2000**, *122*, 1838−1839. (b) Schmidt, A.; Peerless, B.; Dehnen, S. Formation of $[K(18\text{-crown-}6)]_2Bi_2$ and the Influence of 18-crown-6 on the Crystallization of Bismuth-Based Zintl Clusters Obtained From Bi_2^{2-}. *Z. Anorg. Allg. Chem.* **2023**, *649*, No. e202300121.

(42) Zhang, P.; Nabi, R.; Staab, J. K.; Chilton, N. F.; Demir, S. Taming Super-Reduced Bi_2^{3-} Radicals with Rare Earth Cations. *J. Am. Chem. Soc.* **2023**, *145*, 9152−9163.

(43) Pyykkö, P. Additive Covalent Radii for Single-, Double-, and Triple-Bonded Molecules and Tetrahedrally Bonded Crystals: A Summary. *J. Phys. Chem. A* **2015**, *119*, 2326−2337.

(44) Twamley, B.; Sofield, C. D.; Olmstead, M. M.; Power, P. P. Homologous Series of Heavier Element Dipnictenes 2,6-$Ar_2H_3C_6E$ = EC_6H_3-2,6-Ar_2 (E = P, As, Sb, Bi; Ar = Mes = C_6H_2-2,4,6-Me_3; or Trip = C_6H_2-2,4,6-$^iPr_3$) Stabilized by m-Terphenyl Ligands. *J. Am. Chem. Soc.* **1999**, *121*, 3357−3367.

(45) (a) Das, A.; Chen, Y. S.; Reibenspies, J. H.; Powers, D. C. Characterization of a Reactive Rh_2 Nitrenoid by Crystalline Matrix Isolation. *J. Am. Chem. Soc.* **2019**, *141*, 16232−16236. (b) Das, A.; Wang, C. H.; Van Trieste, G. P.; Sun, C. J.; Chen, Y. S.; Reibenspies, J. H.; Powers, D. C. In Crystallo Snapshots of Rh_2-Catalyzed C-H Amination. *J. Am. Chem. Soc.* **2020**, *142*, 19862−19867. (c) Baek, Y.; Das, A.; Zheng, S. L.; Reibenspies, J. H.; Powers, D. C.; Betley, T. A. C-H Amination Mediated by Cobalt Organoazide Adducts and the Corresponding Cobalt Nitrenoid Intermediates. *J. Am. Chem. Soc.* **2020**, *142*, 11232−11243. (d) Van Trieste, G. P.; Reibenspies, J. H.; Chen, Y. S.; Sengupta, D.; Thompson, R. R.; Powers, D. C. Oxygen-

Atom Transfer Photochemistry of a Molecular Copper Bromate Complex. *Chem. Commun.* **2022**, *58*, 12608−12611.
(46) Herzberg, G. Molecular Spectra and Molecular Structure. In *Spectra of Diatomic Molecules*, 2nd ed.; D. Van Nostrand Company Inc., 2013; Vol *1*, pp 194−204.
(47) Mann, J. B.; Meek, T. L.; Allen, L. C. Configuration Energies of the Main Group Elements. *J. Am. Chem. Soc.* **2000**, *122*, 2780−2783.

https://doi.org/10.1021/jacs.4c16830
J. Am. Chem. Soc. 2025, 147, 5330−5339